Heterojunctions

DOI: 10.1002/smll.200600495

Vertically Aligned Zn_2SiO_4 Nanotube/ZnO Nanowire Heterojunction Arrays**

Jun Zhou, Jin Liu, Xudong Wang, Jinhui Song, Rao Tummala, Ning Sheng Xu, and Zhong Lin Wang**

One-dimensional (1D) semiconductor nanostructures are important building blocks for achieving active nanophotonics and nanoelectronics. For example, semiconductor nanowires show great promise for waveguides, nanoelectronic devices, and integrated nanosystems because they can function both as device components for logic, memory, and sensing applications and as interconnects.[1] So far, light-emitting diodes,[2] lasers,[3] photodetectors,[4] and field-effect transistors[5] have been fabricated using semiconductor nanowires. Semiconductor heterostructures[6,7] have played an important role in modern device physics because of their great importance to fundamental research and practical optoelectronic devices.[6c] Unique optical electronic devices, such as single-electron transistors[8]and resonant tunneling diodes,[9] have been constructed based on such heterojunctions between two semiconductors. However, compared to the significant progress in homogeneous nanowires and nanotube preparation, a general synthetic scheme for 1D nanostructure heterojunctions is still lacking. Recently, axial semiconductor heterojunctions with composition modulations have been prepared based on controlled chemical vapor deposition of GaAs/GaP,[7e] InAs/InP,[7c,d] Si/SiGe,[7a] and ZnO/ZnMgO[7b] systems. It has been recognized that the vertically aligned growth of 1D nanostructures is a simple but very efficient self-assembly technique for integrating nanowires into nanodevices. It is of great importance that those hetero-nanostructures can be directly fabricated with aligned morphology while keeping their unique structure and functions.

In this study, we have for the first time been able to prepare aligned Zn_2SiO_4 nanotube/ZnO nanowire heterojunction arrays using a template-assisted growth, followed by an annealing process. The formation of the heterojunction is controlled by the annealing temperature and the size of the ZnO nanowire templates. The technique developed in this paper provides a potential technique for fabricating aligned heterojunction arrays.

The synthesis strategy of the Zn_2SiO_4 nanotube/ZnO nanowire heterojunction arrays involved three steps. First, vertical aligned ZnO nanowire arrays were grown on GaN substrates via a vapor–liquid–solid (VLS) process.[10] Second, an amorphous Si layer was deposited on the surface of the ZnO nanowire arrays by plasma-enhanced chemical vapor deposition (PECVD)[11] to form ZnO/Si core/shell nanowire arrays (see Supporting Information). Finally, these arrays were annealed in an argon atmosphere at $\approx 800\,^{\circ}C$ for 10 h, then at $\approx 900\,^{\circ}C$ for 5 h, to obtain Zn_2SiO_4 nanotube/ZnO nanowire heterojunction arrays.

Figure 1a shows a 30°-tilted scanning electron microscopy (SEM) image of the vertical aligned ZnO nanowire array template, revealing that the ZnO nanowires had an average length of $\approx 8\,\mu m$, and the diameters were in the range of ≈ 50–500 nm. The typical morphology of the Zn_2SiO_4 nanotube/ZnO nanowire heterojunction arrays is shown in Figure 1b (30°-tilted SEM image). The heterostructure exhibited almost the same average length as the ZnO nanowire template. The bottom region of the heterojunctions was very rough, and typically the top region of the heterojunctions had a larger diameter than the bottom region. Figure 1c shows the X-ray diffraction (XRD) pattern of the ZnO nanowire arrays (lower pattern) and the Zn_2SiO_4 nanotube/ZnO nanowire heterojunction arrays (upper pattern). Besides the peaks from the substrate, only diffraction from the (0002) and (0004) atomic planes of ZnO are observed from the ZnO nanowire template, indicating a perfect alignment. Compared to this XRD pattern, two new diffraction peaks were observed from the heterostructures. They were indexed as the (011) and (013) atomic planes of the orthorhombic structured Zn_2SiO_4 (JCPDS card 24-1469: $a = 0.574$ nm, $b = 1.1504$ nm, $c = 0.8395$ nm), respectively.

The detailed morphology and the chemical composition of the Zn_2SiO_4 nanotube/ZnO nanowire heterojunction were characterized by transmission electron microscopy (TEM) and energy-dispersive X-ray spectroscopy (EDX). Figure 2a shows a low-magnification TEM image of two

[*] J. Liu, Dr. X. Wang, J. Song, Prof. Z. L. Wang
School of Materials Science and Engineering
Georgia Institute of Technology
Atlanta, GA 30332-0245 (USA)
Fax: (+1) 404-894-8008
E-mail: zhong.wang@mse.gatech.edu
J. Zhou, Prof. N. S. Xu
School of Physics and Engineering
State Key Lab of Optoelectronic Materials and Technologies
Guangdong Province Key Laboratory of
Display Materials and Technologies
Sun Yat-sen (Zhongshan) University
Guangzhou, 510275 (P. R. China)
Fax: (+86) 208-403-7855
E-mail: stsxns@zsu.edu.cn
J. Liu, Prof. R. Tummala
School of Electrical and Computer Engineering
Georgia Institute of Technology
Atlanta, GA 30332-0245 (USA)

[**] Z.L.W. acknowledges support from NSF grant DMR-9733160, the NASA Vehicle Systems Program and Department of Defense Research and Engineering (DDR&E), and the Defense Advanced Research Projects Agency (Award No. N66001-04-1-8903). N.S.X. acknowledges the support of the project from the National Natural Science Foundation of China, the Ministry of Science and Technology of China, the Education Ministry of China, the Department of Education and Department of Science and Technology of Guangdong Province and Department of Science and Technology of Guangzhou City. J.Z. thanks the Kaisi Fund from Sun Yat-sen University and is grateful for the help from Changshi Lao.

Supporting information for this article is available on the WWW under http://www.small-journal.com or from the author.

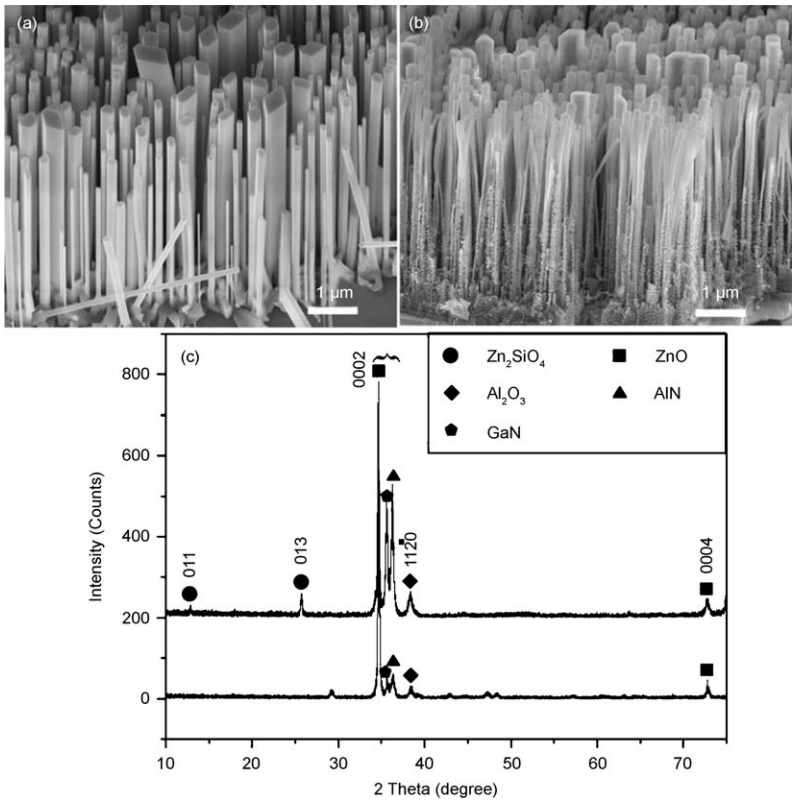

Figure 1. a, b) 30°-tilted SEM images of a ZnO-nanowire array template (a) and a Zn_2SiO_4 nanotube/ZnO nanowire heterojunction array (b); c) XRD patterns of the ZnO-nanowire array template (upper pattern) and the Zn_2SiO_4 nanotube/ZnO nanowire heterojunction array.

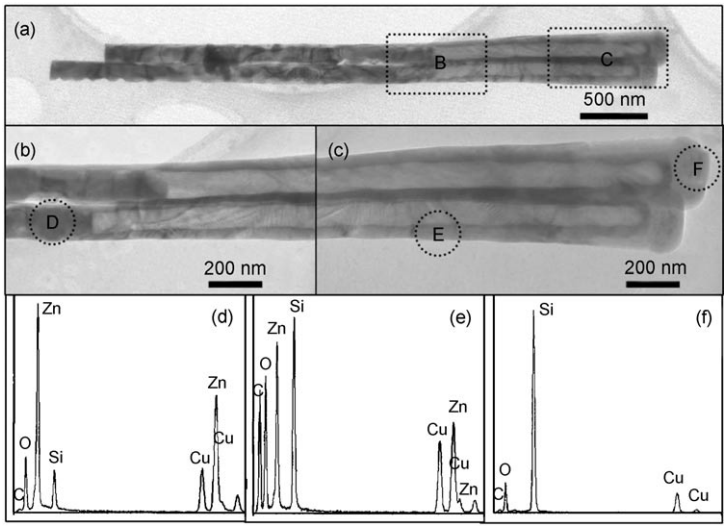

Figure 2. a) Low-magnification TEM image of two Zn_2SiO_4 nanotube/ZnO nanowire heterojunctions; b, c) enlarged TEM images of the rectangular-enclosed areas B and C in (a); d–f) EDX spectra taken from the circled areas D, E, and F in (b) and (c).

Zn_2SiO_4 nanotube/ZnO nanowire heterojunctions. Enlarged TEM image of the rectangular-enclosed area of B and C in Figure 2a are shown in Figure 2b and c, respectively, revealing the nanotube/nanowire character of the heterojunctions. The diameter of the nanotube region is larger than nanowire region, which agrees with the SEM observation (Figure 1b). Figure 2d shows the EDX spectrum taken from the circled area D in Figure 2b. Besides the Cu and C signal from the TEM grid, Zn, O, and Si were detected. The same elements (Figure 2e) were detected from the nanotube wall (circled area E in Figure 2c), although the Si/Zn ratio increased significantly. No Zn signal (Figure 2f) was detected from the top end of the nanowire heterojunction (circled area F in Figure 2c).

Figure 3a shows a typical TEM image of an individual Zn_2SiO_4 nanotube/ZnO nanowire heterostructure. The nanotube section and nanowire section can be clearly identified by the enlarged TEM image shown in Figure 3b. The surface of the nanowire's bottom end was very rough. The detailed internal microstructure of the Zn_2SiO_4 nanotube/ZnO nanowire heterojunction was carefully studied by high-resolution TEM and selected-area electron diffraction (SAED) pattern analysis. The inset of Figure 3c is a SAED pattern taken from the nanowire section. One set of diffraction spots can be indexed as hexagonal ZnO with a $[\bar{2}2\bar{1}0]$ zone axis. The other weak diffraction spots were contributed by the Zn_2SiO_4 crystal. The corresponding HRTEM image (Figure 3c) is consistent with the SAED pattern analysis. The fringes, with an interplanar spacing of $\approx$0.26 nm (corresponding to the (0002) plane of hexagonal ZnO), are perpendicular to the axis direction. The discrete crystalline outer layer can be attributed to Zn_2SiO_4. By tilting the TEM grid by $\approx$4.3°, another SAED pattern from the nanotube section was acquired. The diffraction spots can be indexed as orthorhombic Zn_2SiO_4 with a $[3\bar{1}0]$ zone axis, indicating the nanotube is single crystalline. The lattice fringes

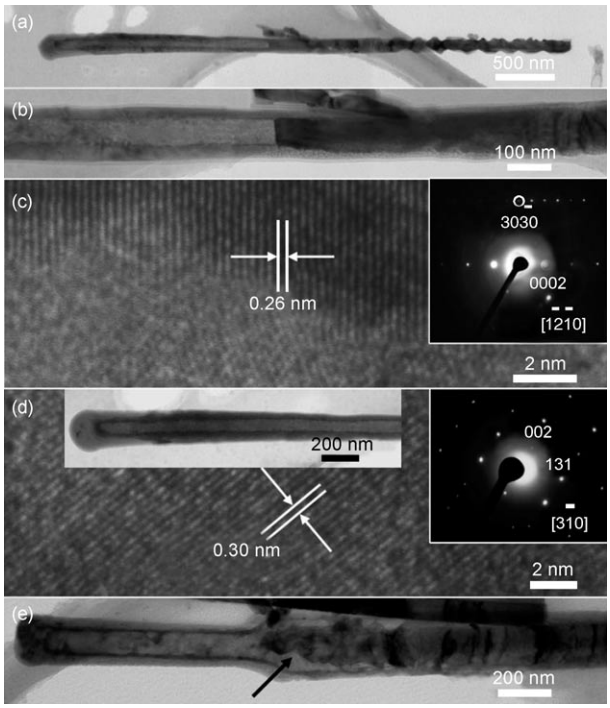

Figure 3. a) Low-magnification TEM image of a single Zn_2SiO_4 nanotube/ZnO nanowire heterojunction; b) enlarged TEM image of the heterojunction shown in (a); c, d) HRTEM images and corresponding SAED patterns of the nanowire and nanotube sections of the heterojunction, respectively; e) low-magnification TEM image of a section of a heterojunction indicating that the ZnO core (arrow) was evaporated from the top end.

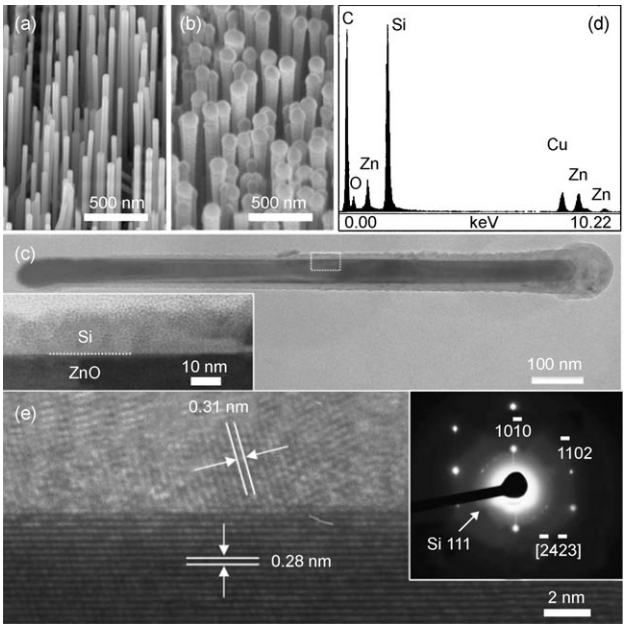

Figure 4. a, b) 30°-tilted SEM images of a ZnO-nanowire array template (a) and a ZnO/Si core/shell nanowire array (b), respectively; c) typical TEM image of a single ZnO/Si core/shell nanowire. The inset is a enlarged TEM image; d) EDX spectrum of the ZnO/Si core/shell nanowire shown in (c); e) HRTEM image and corresponding SAED pattern of the ZnO/Si core/shell nanowire.

in Figure 3d, with a d spacing of $\approx$0.3 nm, can be identified as the $(13\bar{1})$ plane of orthorhombic Zn_2SiO_4.

In our study, we found that the formation of the Zn_2SiO_4 nanotube/ZnO nanowire heterojunction can be controlled by the size of the ZnO nanowire template and the annealing temperature. For example, when small-sized ZnO nanowires (average length of $\approx$1 μm, average diameter of $\approx$40 nm) were used as a template, while the other parameters (such as the PECVD growth parameters, annealing temperature, and annealing time) were kept constant, Zn_2SiO_4 nanotube arrays were prepared (see Supporting Information). In contrast, lower annealing temperatures ($\approx$700 °C) gave ZnO/Si core/shell nanowire arrays, as shown in Figure 4. Figure 4a b are 30°-tilted SEM images of ZnO nanowire template and ZnO/Si core/shell nanowire arrays, respectively, showing that an aligned morphology was very well preserved after Si coating. Figure 4c is a typical TEM image of a single ZnO/Si core/shell nanowire with a length of $\approx$1 μm. The contrast clearly shows the core/shell structure of the nanowire. The Si shell and the sharp Si/ZnO interface were shown in the inset of Figure 4c. The thickness of the Si shell was not uniform, and decreased from the top to the bottom. A HRTEM image reveals the crystal structure at the interface, as shown in Figure 4e. The lattice fringes of the core, with a spacing of $\approx$0.28 nm, can be attributed to the $(10\bar{1}0)$ plane of hexagonal ZnO, and the lattice fringes of the shell, with a spacing of $\approx$0.31 nm, can be attributed to the (111) plane of face-centered cubic (fcc) Si. The distinguishing crystal structures indicate that there was no reaction between the Si shell and ZnO core. The corresponding SAED pattern is shown in the inset of Figure 4d. A set of diffraction spots can be indexed as hexagonal ZnO with a $[\bar{2}4\bar{2}3]$ zone axis. In addition, the diffraction rings in the SAED pattern can be attributed to the (111) plane of Si.

The formation mechanism of the nanotube/nanowire heterojunction was based on the chemical reactions between Si, O_2, and ZnO. During the annealing process, the thin Si shell reacted with the residual oxygen in the chamber and quickly formed amorphous SiO_2:

$$Si(s) + O_2(v) \rightarrow SiO_2(s) \quad (1)$$

SiO_2 then reacted with the ZnO core and formed Zn_2SiO_4 around the interface:

$$SiO_2(s) + 2\,ZnO(s) \rightarrow Zn_2SiO_4(s) \quad (2)$$

The consumption of ZnO left a small open area between the Zn_2SiO_4 shell and the ZnO core. The vacuum in this open area facilitated the decomposition of the rest of the ZnO nanowire core to yield Zn vapor and O_2 vapor at a high temperature of $\approx$800–900 °C:

$$ZnO(s) \leftrightarrow Zn(v) + O_2(v) \quad (3)$$

If the Zn_2SiO_4 shell is thin enough, Zn and O_2 are able to diffuse through it and react with the remaining SiO_2 to form more Zn_2SiO_4:

$$SiO_2(s) + Zn(v) + O_2(v) \rightarrow Zn_2SiO_4(s) \quad (4)$$

This reaction leads to a thicker Zn_2SiO_4 shell. During the annealing process, reactions (2) and (4) are two possible pathways for forming the Zn_2SiO_4 shell. It was likely that reaction (2) occurred first between the solid SiO_2 shell and the ZnO core around the interface. The consumption of ZnO in reaction (2) would leave a small open space at the interface region. Vacuum in this small space and the high local temperature can initiate the decomposition of ZnO core following reaction (3). Therefore, this small open space was quickly filled up with Zn and O_2 vapors, which would diffuse into the SiO_2 shell forming more Zn_2SiO_4 following reaction (4). The consumption of Zn and O_2 vapor would keep driving reaction (3) to the right-hand side. Therefore, we can assume that the formation of Zn_2SiO_4 was initiated by reaction (2) and followed by reaction (4). Once the entire SiO_2 shell was transformed into Zn_2SiO_4, no more Zn and O_2 could be consumed and the decomposition of the ZnO core stopped forming the heterojunction structure. On the other hand, if the ZnO core could not provide enough Zn and O_2 to completely convert the SiO_2 shell, the entire ZnO core would be used up and the result is a tubular structure. In addition, it was most likely that the initiation reaction (reaction (2)) was more easily started at locations with higher interface energy, such as the corner of the nanowire tip. As a result, a sharp tip of the ZnO core could always be observed at the tube/wire interface, as shown in Figure 3e.

When the Si shell was very thin, such as around the bottom area of the ZnO/Si core/shell nanowire (Figure 4c), there was not enough Si to react with the entire ZnO core. Thus when reaction (4) occurs, textured islands on the surface of ZnO were formed instead of continuous single-crystalline layer due to the large lattice mismatch between ZnO and Zn_2SiO_4.[1] Therefore, there are open areas on the ZnO nanowire surface that are not covered by the Zn_2SiO_4. The evaporation of ZnO from these open areas may cause the rough surface of the ZnO nanowires (Figures 1b and 3a).

It is well known that Zn_2SiO_4 is a widely used in industry as a green-luminescent material and ZnO exhibits near-UV luminescence. Figure 5 shows a representative photoluminescence (PL) spectrum of the ZnO-nanowire array template (upper line) and the Zn_2SiO_4 nanotube/ZnO nanowire heterojunction arrays (lower line). The spectra clearly displayed a sharp and strong near-UV luminescence peak at ≈379 nm with a full width at half-maximum (FWHM) of 14.9 nm, which can be attributed to ZnO. In comparison, the PL spectrum of the heterojunction arrays shows a weak and broad green emission peak, centered at ≈532 nm (inset of Figure 5), which was attributed to Zn_2SiO_4, and is consistent with previous reports.[12–15]

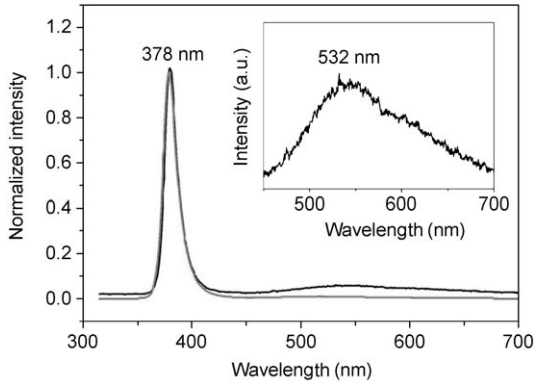

Figure 5. PL spectra of the ZnO-nanowire array template (top curve) and the Zn_2SiO_4 nanotube/ZnO nanowire heterojunction array (lower curve). The inset is an enlarged spectrum showing the luminescence peak due to Zn_2SiO_4.

In summary, we have fabricated Zn_2SiO_4 nanotube/ZnO nanowire heterojunction arrays by using ZnO nanowire arrays as the template; the as-synthesized heterojunctions were crystalline. The thermal decomposition of ZnO initiated from the tip of the nanowire, and the annealing time, temperature, and the thickness of the initial Si coating are the key parameters for controlling the formation of the nanotube/nanowire heterojunctions. This technique demonstrates a potential technique for fabricating aligned heterojunction arrays.

Experimental Section

Synthesis of vertical aligned ZnO nanowires arrays: An undoped, *c*-plane-oriented GaN film with a thickness of 2 μm (with an AlN film as a buffer layer) was grown on an *a*-plane sapphire single-crystal substrate and then used as the substrate for our experiments. A ≈2-nm-thick gold catalyst layer was deposited on the substrate with a thermal evaporator. ZnO nanowires were grown through a VLS process using a mixture of equal amounts (by mass) of ZnO and graphite powders (0.6 g each) that was placed in the close end of an small quartz tube (inner diameter 1.8 cm). Then the quartz tube was loaded into an alumina tube (150 cm long, 4 cm inner diameter). With the closed end at the center of the alumina tube, the substrate was placed 12.5 cm away from the source material at the open end of the small quartz tube, which is on the downstream side. Then the alumina tube was placed in a horizontal tube furnace (model F79345 from Barnstead/Thermolyne Co.). After the system was pumped down to $\approx 2 \times 10^{-2}$ mbar, argon was used as a carrier gas at a flow rate of 49 sccm with an additional 2% (1 sccm) of oxygen to facilitate the reaction; the working pressure was ≈200 mbar. The furnace was then heated to 950 °C at a heating rate of 50 °C min^{-1} and held at the peak temperature for 30 min. Finally, the system was slowly cooled down to room temperature.

Synthesis of ZnO/amorphous Si core/shell nanowires: ZnO/amorphous Si core/shell nanowires were prepared by plasma-enhanced chemical vapor deposition (PECVD). The PECVD chamber was firstly pre-pumped to 10 mTorr. SiH_4 gas was then injected into the chamber at a flow rate of ≈5 sccm, and the pressure of the chamber was maintained at ≈300 mTorr. PECVD was then carried out at a power of 50 W, with the precursors in a plasma state under the rf operating voltage. Amorphous Si was deposited on the surface of the ZnO nanowires at a temperature of ≈300 °C for 5 min. Eventually, ZnO/amorphous Si core/shell nanowires were formed.

Synthesis of Zn_2SiO_4 nanotube/ZnO nanowire heterojunction arrays: ZnO/amorphous Si core/shell nanowire arrays were then

annealed in the horizontal tube furnace. Before the annealing process, the system was firstly pumped down to $\approx 2 \times 10^{-2}$ mbar, argon gas at a flow rate of 50 sccm was introduced into the system, and the working pressure was ≈ 150 mbar. The furnace was then heated to $\approx 800\,^{\circ}C$ with a heating rate of $50\,^{\circ}C\,min^{-1}$ and held at that temperature for 10 h. The furnace was then ramped to $\approx 900\,^{\circ}C$ and maintained at that temperature for another 5 h. Finally, the system was slowly cooled down to room temperature.

Characterization: The products were characterized by high-resolution field-emission scanning electron microscopy (FESEM: LEO 1530 FEG at 10 kV) and transmission electron microscopy (TEM; Hitachi 2000 at 200 kV), energy dispersive X-ray spectroscopy (EDX), and X-ray diffraction (XRD; Philips PW 1800 with Cu Kα radiation). The photoluminescence properties of the ZnO nanowire arrays and Zn_2SiO_4 nanotube/ZnO nanowire heterojunction arrays were measured at room temperature using a 266-nm Nd:YAG Q-switched laser with an average power of 1.9 mW as the excitation light source.

Keywords:
arrays · heterojunctions · nanowires · template synthesis · zinc oxide

[1] a) Y. Huang, X. Duan, Y. Cui, L. J. Lauhon, K. Kim, C. M. Lieber, *Science* **2001**, *294*, 1313; b) A. Bachtold, P. Hadley, T. Nakanishi, C. Dekker, *Science* **2001**, *294*, 1317.

[2] a) X. Duan, Y. Huang, Y. Cui, J. Wang, C. M. Lieber, *Nature* **2001**, *409*, 66; b) H. M. Kim, T. W. Kang, K. S. Chung, *Adv. Mater.* **2003**, *15*, 567; c) Z. Zhong, F. Qian, D. Wang, C. M. Lieber, *Nano Lett.* **2003**, *3*, 343; d) H. Kim, Y. Cho, H. Lee, S. Kim, S. R. Ryu, D. Y. Kim, T. W. Kang, K. S. Chung, *Nano Lett.* **2004**, *4*, 1059; e) O. Hayden, A. B. Greytak, D. C. Bell, *Adv. Mater.* **2005**, *17*, 701.

[3] a) M. H. Huang, S. Mao, H. Feick, H. Yan, Y. Wu, H. Kind, E. Weber , R. Russo, P. Yang, *Science* **2001**, *292*, 1897; b) J. Johnson, H. Choi, K. P. Knutsen, R. D. Schaller, P. Yang, R. J. Saykally, *Nat. Mater.* **2002**, *1*, 106; c) X. Duan, Y. Huang, R. Agarwal, C. M. Lieber, *Nature* **2003**, *421*, 242; d) R. Agarwal, C. J. Barrelet, C. M. Lieber, *Nano Lett.* **2005**, *5*, 917; e) C. H. Liu, J. A. Zapien, Y. Yao, X. M. Meng, C. S. Lee, S. S. Fan, Y. Lifshitz, S. T. Lee, *Adv. Mater.* **2003**, *15*, 838.

[4] J. Wang, M. S. Gudiksen, X. Duan, Y. Cui, C. M. Lieber, *Science* **2001**, *293*, 1455.

[5] a) Y. Cui, C. M. Lieber, *Science* **2001**, *291*, 851; b) M. Arnold, P. Avouris, Z. W. Pan, Z. L. Wang, *J. Phys. Chem. B* **2003**, *107*, 659; c) Y. Cui, Z. Zhong, D. Wang, W. U. Wang, C. M. Lieber, *Nano Lett.* **2003**, *3*, 149.

[6] a) H. J. Choi, J. H. Shin, K. Suh, H. K. Seong, H. C. Han, J. C. Lee, *Nano Lett.* **2005**, *5*, 2432; b) F. Qian, S. Gradecak, Y. Li, C. Y. Wen, C. M. Lieber, *Nano Lett.* **2005**, *5*, 2287; c) H. M. Lin, Y. L. Chen, J. Yang, Y. C. Liu, K. M. Yin, J. J. Kai, F. R. Chen, L. C. Chen, Y. F. Chen, C. C. Chen, *Nano Lett.* **2003**, *3*, 537; d) D. H. Zhang, Z. Q. Liu, S. Han, C. Li, B. Lei, M. P. Stewart, J. M. Tour, C. W. Zhou, *Nano Lett.* **2004**, *4*, 2151; N. Sköld, L. S. Karlsson, M. W. Larsson, M. E. Pistol, W. Seifert, J. Trägårdh, L. Samuelson, *Nano Lett.* **2005**, *5*, 1943.

[7] a) Y. Y. Wu, R. Fan, P. D. Yang, *Nano Lett.* **2002**, *2*, 83; b) W. I. Park, G. C. Yi, M. Kim, S. J. Pennycock, *Adv. Mater.* **2003**, *15*, 526; c) B. J. Ohlsson, M. H. Magnusson, M. T. Björk, L. R. Wallenberg, K. Deppert, L. Samuelson, *Appl. Phys. Lett.* **2001**, *79*, 3335; d) M. T. Björk, B. J. Ohlsson, T. Sass, A. I. Persson, C. Thelander, M. H. Magnusson, K. Deppert, L. R. Wallenberg, L. Samuelson, *Nano Lett.* **2002**, *2*, 87; e) M. S. Gudiksen, L. J. Lauhon, J. Wang, D. C. Smith, C. M. Lieber, *Nature* **2002**, *415*, 617.

[8] C. Thelander, T. Mårtensson, M. T. Björk, B. J. Ohlsson, M. W. Larsson, L. R. Wallenberg, L. Samuelson, *Appl. Phys. Lett.* **2003**, *83*, 2052.

[9] M. T. Björk, B. J. Ohlsson, C. Thelander, A. I. Persson, K. Deppert, L. R. Wallenberg, L. Samuelson, *Appl. Phys. Lett.* **2002**, *81*, 4458.

[10] a) X. D. Wang, J. H. Song, P. Li, J. H. Ryou, R. D. Dupuis, C. J. Summers, Z. L. Wang, *J. Am. Chem. Soc.* **2005**, *127*, 7920; b) J. H. Song, X. D. Wang, E. Reido, Z. L. Wang, *J. Phys. Chem. B* **2005**, *109*, 9869; c) X. D. Wang, J. H. Song, C. J. Summers, J. H. Ryou, P. Li, R. D. Dupuis, Z. L. Wang, *J. Phys. Chem. B* **2006**, *110*, 7720.

[11] J. Zhou, J. Liu, R. S. Yang, C. S. Lao, P. X. Gao, R. Tummala, N. S. Xu, Z. L. Wang, *Small*, **2006**, *2*, 1344.

[12] X. D. Wang, C. J. Summers, Z. L. Wang, *Adv. Mater.* **2004**, *16*, 1215.

[13] L. W. Yang, X. L. Wu, G. S. Huang, T. Qiu, Y. M. Yang, G. G. Siu, *Appl. Phys. A* **2005**, 81, 929.

[14] X. Feng, X. L. Yuan, T. Sekiguchi, W. Z. Lin, J. Y. Kong, *J. Phys. Chem. A* **2005**, *109*, 15786.

[15] L. M. Xiong, J. L. Shi, J. L. Gu, W. H. Shen, X. P. Dong, H. R. Chen, L. X. Zhang, J. H. Guo, M. L. Ruan, *Small* **2005**, *1*, 1044.

Received: September 13, 2006
Revised: December 1, 2006
Published online on February 19, 2007

